Supporting Information

Flexible artificially networked structure for ambient/high pressure solar steam generation

Seyed Mohammad Sajadi†, Nazanin Farokhnia†,Peyman Irajizad, Munib Hasnain, and Hadi Ghasemi

† Equal Contributor

1. Synthesis of the flexible artificially networked structure for steam generation

The Polydimethylsiloxane (PDMS) was obtained from Cone Elastomer (Kit 184SIL). The hardener in the ratio of 1:10 was added to the PDMS and mixed thoroughly. We used the internal phase emulsion approach to develop a highly porous PDMS skeleton. Brine with 1:1 ratio is added to PDMS and thoroughly mixed to make a saturated emulsion. The diameter of the dispersed water droplets in the emulsion varies in a wide range of length-scale. These droplets leave the structure through evaporation in polymerization process leading to a highly porous polymer skeleton (see Fig. S1). The acid-washed graphite flakes are obtained from Ashbury Carbons with product number of 3772. These flakes were heated in a microwave for 10-15s to achieve high-surface area fluffy exfoliated graphite. Further treatment with microwave did not affect hydrophilicity of the graphite flakes. The trapped gases between the graphite layers expand in the heating process and detach the flakes from each other. The volumetric exfoliation during this process is approximately 100 times. The fabricated graphite was added to the PDMS solution and mixed in the ratio given in Table 1. To achieve highly-interconnected artificial veins in the structure, we used scarifying aluminum foam. The aluminum foam was purchased form K. R. Reynolds company (Duocel Aluminum Foam). Three types of the foam were examined in this work, 20 PPI and 40 PPI (pore per inch) with different density as shown in Table 1. The foam was impregnated with the developed solution of graphite and PDMS. The foam was placed in the oven for one hour at 110 ^{o}C.

After curing of the PDMS skeleton, the aluminum foam was dissolved by soaking the structure in hydrochloric acid (HCL) 35-38%. The dissolving process takes around 48-72 hrs. The final structure was washed with distilled water.

Table 1. Specification of the studied flexible artificially networked structures

Sample	PDMS [mL]	Brine [mL]	Graphite [mg]	Aluminum Foam
S1	5.5	5.5	0.2	40 PPI (7-9% Density)
S2	5.5	5.5	0.2	20 PPI (13-15% Density)
S3	5.5	5.5	0.2	20 PPI (7-9% Density)

2. Development of the Porous Polymer Skeleton

The highly porous PDMS skeleton is developed through high internal phase emulsion approach. To show the scale of porosity through this approach, we fabricated the samples of pure porous PDMS as shown in Fig. S1. This structure is achieved through mixing of brine and PDMS with ratio of 1:1. The mixed solution is cured in the oven at 110 ^{o}C for one hr.

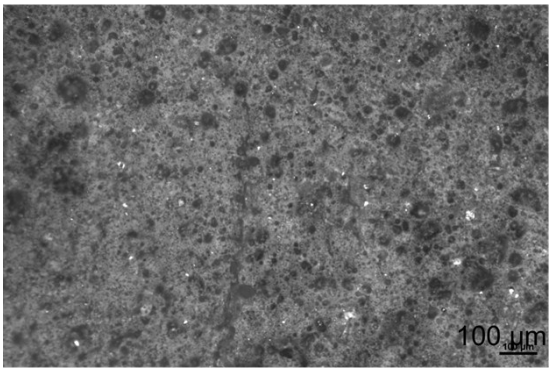

Fig. S1. The structure of porous PDMS is shown. The structure includes pore sizes in the range of 2-100 µm. These pores make the structure buoyant and reduce its thermal conductivity.

3. Porosity Measurements

We used fluid saturation approach to measure porosity of the structure. First, the mass of the dry sample was measured (m_1). Next, we filled the structure with isopropyl alcohol and measured the saturated mass of the structure (m_2). Low surface tension of isopropyl alcohol allows for complete wetting of the veins inside the structure. The mass of fluid in the pores is written as ($m_p=m_2-m_1$). Then, volume of the pores is written as $V_p= m_p/\rho_{iso}$, where ρ_{iso} denotes the density of isopropyl alcohol (792 kgm^{-3}). In the third step, we immersed the saturated structure in a bath of isopropyl alcohol and measured the buoyancy force imposed on the structure (W_3). The choice of isopropyl alcohol allows the structure to become completely immersed in the bath to avoid any uncertainty in the buoyancy force measurements. The volume of the structure (V_s) is written as

$$V_s = \frac{W_3/g}{\rho_{iso}}$$

Thus, the porosity of the structure is written as

$$Porosity = \frac{V_p}{V_s}$$

We measured the porosity of S3 structure in five independent measurements. The measured porosity is 53 ± 3 %.

4. Dynamics of Wetting

The dynamic wetting of the structure is examined through high-speed imaging of a droplet interaction with the material structure. The high-speed camera (Phantom V711, vision research) is utilized in these experiments. Once a porous structure with positive imbibition parameter (i.e. hydrophilic surface) comes in contact with a fluid, the fluid impregnates quickly in the structure. The dynamics of the fluid flow to the structures is divided into two regimes: (i) inertia dominant region and (ii) viscous dominant region. This dynamics depends on radius of the channels in the structure, interfacial properties of the solid and liquid and the

hydrodynamic properties of the fluid. We have used this dynamics to determine the average size of the interconnected veins in the structure. We placed a water droplet on the surface of the structure and examined its dynamic as shown in Fig. 2b. A movie of the droplet interaction with the material structure at 30 frame/s is included (Movie 1). We consider that the fluid flow in the structure is mostly viscous dominant and use the Washburn's law to determine the average size of the veins in the structure written as

$$z^2(t) = \frac{1}{2}\frac{\gamma R\cos\theta}{\mu}t \quad (1)$$

where z denotes the length-scale of impregnation, γ liquid-vapor surface tension, R the average dimension of the channels, θ contact angle, and μ the viscosity of the fluid. We determined the impregnation length through the volume of the droplet divided by the wetted area. Also, the contact angle of the water on the exfoliated graphite surface measured in Ghasemi et al.[27] is 40°. The average size of the channels is 30 ± 10 μm. Also, we can take the derivative of the Washburn's law to calculate the velocity of the fluid once it reaches the surface of the structure. This velocity is ~ 10 cm/s. If we consider no change in the interfacial properties at high solar illumination, the maximum electromagnetic illumination on the surface without drying is written as

$$\dot{q} = h_{fg}\,\rho\,V \quad (2)$$

where $\dot{q}$ denotes the electromagnetic flux, h_{fg} enthalpy of phase change, ρ density of fluid, and V velocity of fluid in the veins at the surface of the structure. Thus, the structure can sustain the fluid flow to the surface even up to high intensity of electromagnetic illumination in order of 10^5 kWm^{-2} without drying.

5. Thermal Conductivity Measurements

Thermal conductivity of the structure is measured through IR method. In this approach, the structure is sandwiched between two reference glass slabs with known thermal conductivity. A resistance heater is attached to the top glass slab and the current through the heater is tuned

to introduce a range of temperature gradient across the sample. The setup is placed in front of an IR camera with resolution of 25 μm to measure the temperature gradient in the glass slabs and the sample. The IR camera is calibrated by measurement of the emissivity map in an isothermal condition. As the thermal conductivity of the reference material is known, the measured temperature gradient in the glass slab is used to determine the heat flux to the sample. Given the heat flux and the temperature gradient in the material, thermal conductivity of the material is determined through Fourier equation. The linear correlation of heat flux and temperature gradient suggests a negligible contribution of convection losses by the sides in the measurements.

6. Chemical Stability of the Material Structure

To examine the chemical stability of structure, we prepared a range of solutions in PH range of 1-11. The acidic solutions are prepared through various HCL and water concentrations. The basic solutions are Tris 0.15 mM NaCL (PH=8) and Sodium Phosphate (PH=11) solutions. We soaked the structure in these solutions for 18 hrs. Figure S2 shows the structure before and after each experiment. No change in the integrity of the structure is observed.

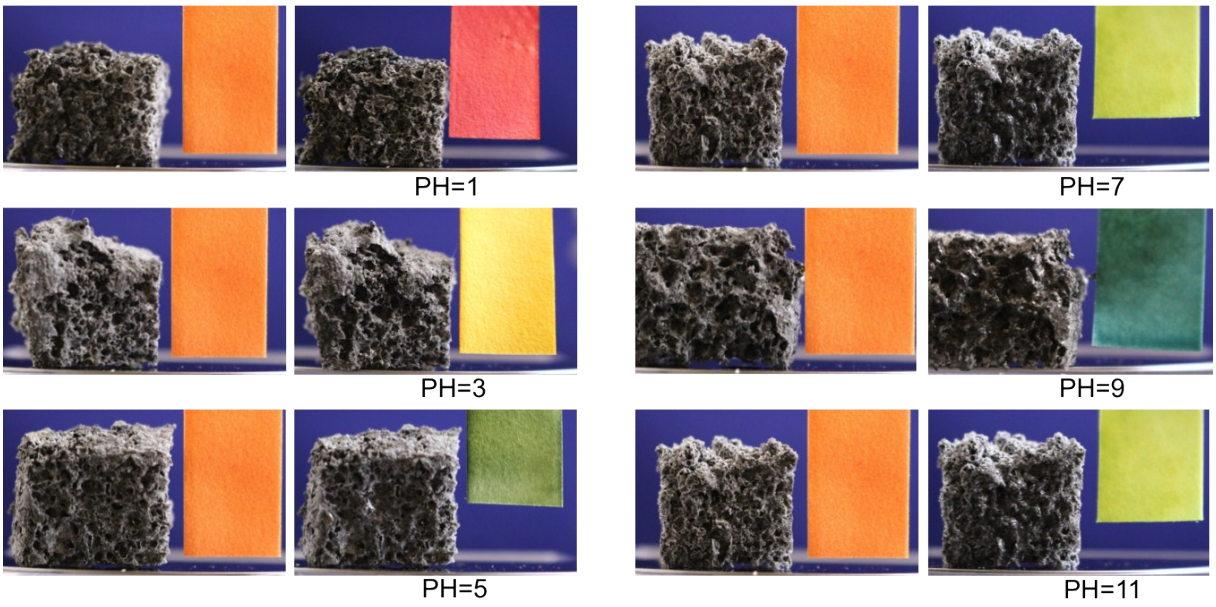

Fig. S2. The developed material structure was examined in a range of chemical solutions with the PH range of 1-11. The structure before and after each experiment is shown. No change in the integrity of the structure was observed.

7. Experimental Setup

The experimental setup in this work is specifically designed to assess performance of the structure at low and high steam pressures. As shown in Fig. S3, the experimental setup includes (1) a cylindrical chamber with diameter of 25.4 mm with an attached flange on top; (2) the glass flange (Archon Industries, tempered borosilicate glass) that can withstand up to high pressure of 40 bar; (3) a solar simulator equipped with an optical head with maximum concentration of 50 kWm^{-2}, (OAI 0131-0293-01 with Aluminum mirror and 1.6 kW lamp); (4) a power measurement system consisting of a Newport thermopile detector (919P-500-65, 500W, 65 mm diameter) and Newport power meter (1918-R); (5) thermocouples type T for measurement of liquid and vapor temperatures, (6) A pressure gauge (Prosense, SPT25-20-0500A) to measure the pressure of the generated steam, (7) a syringe pump (Kd Scientific) to supply the liquid to the chamber; (8) and a data acquisition system (National Instruments, NI USB-6210).

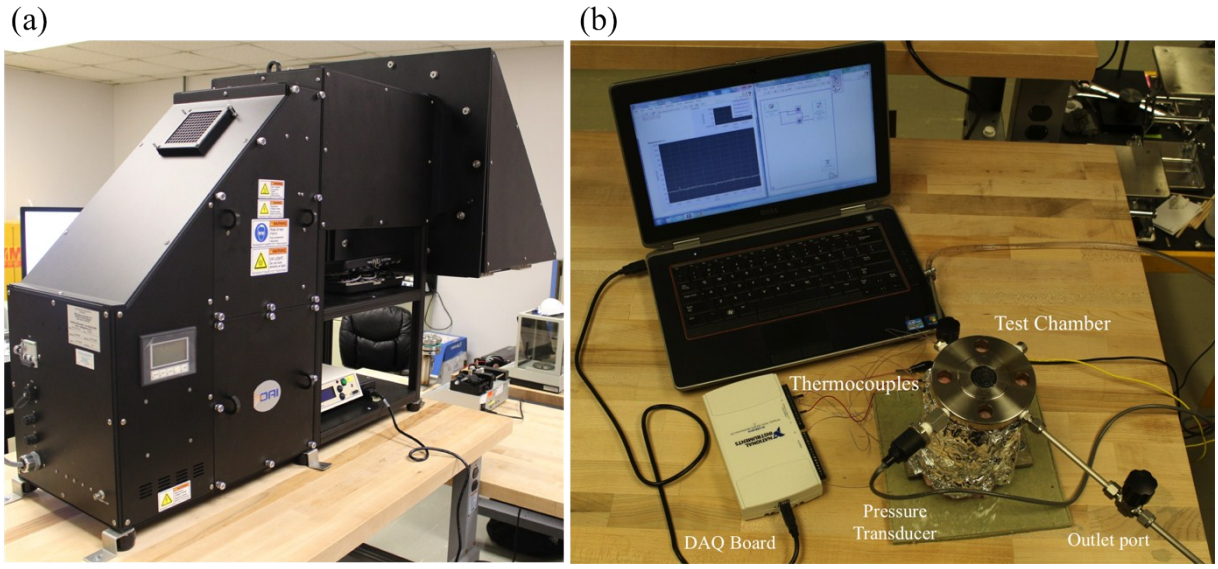

Fig. S3. The experimental setup for ambient and high-pressure solar steam generation. (a) The solar simulator with the optical head enables us to conduct the experiments in the solar concentration range of 1-50 kWm^{-2}. (b) The measurement instrument and the test chamber are shown.

The cylindrical chamber is covered with fiberglass insulation to minimize the 2D side losses. The chamber has one inlet and one outlet. The inlet of the chamber is connected to the syringe pump through a piping system. The outlet of the chamber is left open for removal of generated steam. The syringe pump provides the ability to measure the evaporation rate of water accurately in a steady-state condition. The thermocouples and pressure gauge are calibrated before the experiments. The thermocouple in the vapor phase is placed at approximately 1 mm on top of the structure. This thermocouple is coated with a white coating to suppress the effect of direct illumination on the temperature measurements. The thermocouples in the liquid phase are placed underneath of the structure with intervals of 15 mm. All the thermocouples and the pressure gauge are connected to the Data Acquisition system and the generated data is collected by a LabView program. The solar intensity at the surface of the structure is measured with the Newport thermopile. Each measurement of the solar intensity is repeated three times and the average measured value is reported. The

standard deviation in the measurements of solar irradiation is less than 2%. We have used a highly reflective aperture with diameter of 25 mm on top of the test chamber to form a circular solar illumination spot with the same inside diameter of test chamber. All the experiments were conducted for long time to reach steady-state condition.

8. Parasitic Heat Losses by the Experimental Setup

The parasitic loss of the experimental setup is determined through simulation in COMSOL. The temperature of the generated steam at ambient pressure for pure graphite and DLS is shown in Fig. S4. In all the structures, the generated steam reaches to 100 ^{o}C. The energy dissipated through surface convection, radiation, and heat losses to the experimental setup is only a function of structure temperature (i.e. close to steam temperature) and will be the same for all the structures. The difference between the performances of different structures is heat dissipated to the underlying liquid.

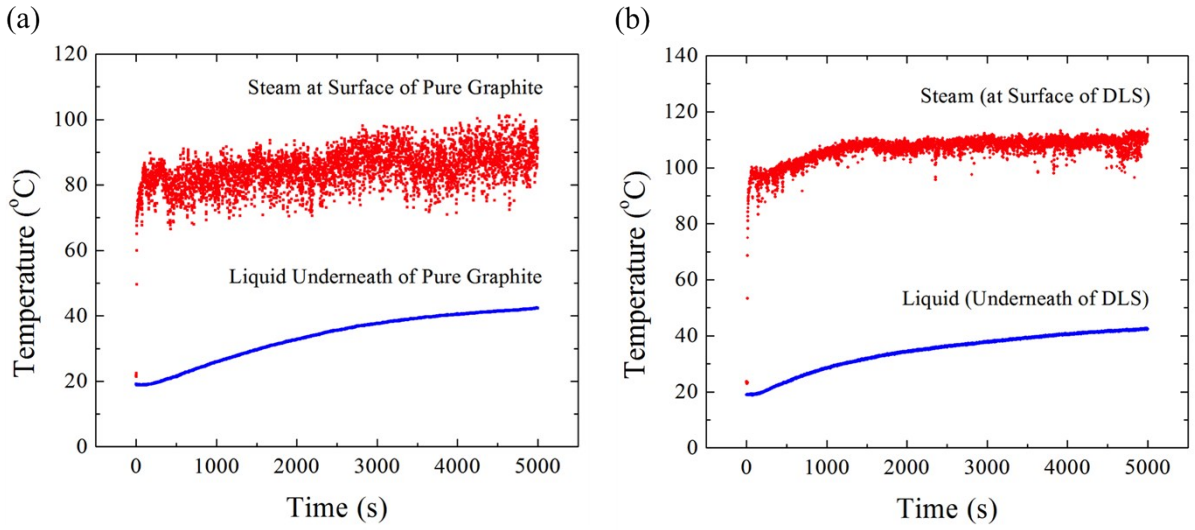

Fig. S4. Temperature of the generated steam and underlying liquid for different structures are shown. For both pure graphite and DLS, the generated steam reaches to temperature of 100 ^{o}C. However, DLS has shorter transient time.

Assuming the temperature of top of the structure is close to the steam temperature, we have determined heat dissipated to the experimental setup through the simulations. The simulated temperature map of the experimental setup is shown in Fig. S5. The boundary condition in

these simulations is convective heat transfer with coefficient of 10 $Wm^{-1}K^{-1}$. These simulations suggest that the experimental setup imposes the parasitic losses in the range of 38-44% under the solar concentration range of 12-40 kWm^{-2}.

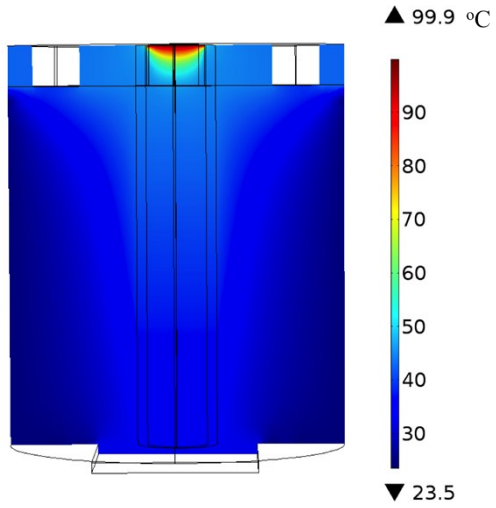

Fig. S5. The temperature map of the cross-section of the experimental setup is shown. This experimental setup imposes up to 44% parasitic heat loss in the solar steam generation experiments.

9. Energy Dissipation to the Bulk Liquid

As discussed above, the thermocouples in the bulk liquid were implemented to determine the energy dissipation to the underlying liquid. The transient temperature of liquid below the structure (< 2 mm gap between the thermocouple and the bottom of the structure) is compared between the developed structure herein and the other state-of-the-art structures. Lower temperature rise of the liquid is equivalent to better heat localization by the structure and consequently more efficient steam generation. These temperature trends are shown at various solar irradiations powers in Fig. S6.

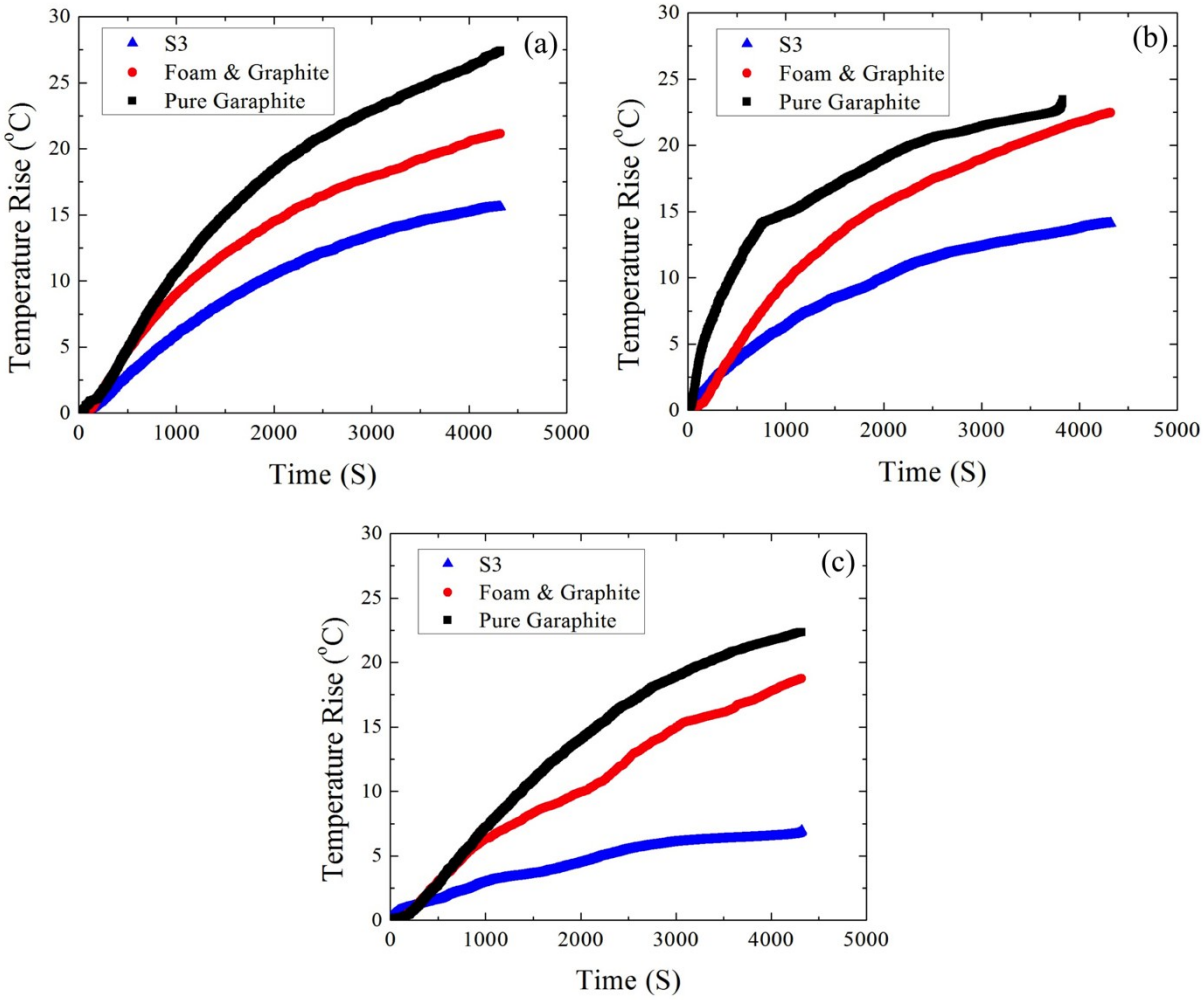

Fig. S6. Temperature rise of the liquid below the structure is shown for different state-of-the-art structures at different solar irradiation power (a) 40 kWm^{-2}, (b) 30 kWm^{-2}, (c) 20 kWm^{-2}. Lower temperature rise indicates more heat localization by the structure and consequently higher efficiency of steam generation.